ELSEVIER

Contents lists available at ScienceDirect

Ceramics International

journal homepage: www.elsevier.com/locate/ceramint





Effect of substrate rotational speed during deposition on the microstructure, mechanical and tribological properties of a-C:Ta coatings

Mingming Yan a,b , Cong Wang a,b , Xudong Sui a,b,c , Jian Liu a,b,c , Yan Lu a,b,c,* , Junying Hao a,b,c,** , Weimin Liu a,b

- a State Key Laboratory of Solid Lubrication, Lanzhou Institute of Chemical Physics, Chinese Academy of Science, Lanzhou, 730000, China
- b Center of Materials Science and Optoelectronics Engineering, University of Chinese Academy of Sciences, Beijing, 100049, China
- ^c Qingdao Center of Resource Chemistry and New Materials, Qingdao, 266000, China

ARTICLE INFO

Keywords: Composite coatings Rotational speed Friction coefficient Wear rate

ABSTRACT

Rotational speed has an important influence on the performance of coating materials. The a-C:Ta composite coatings were prepared by controlling the substrate rotational speed during deposition process using PVD technique. The results showed that the coating transformed from dense structure to columnar structure. Due to the changes of deposition time and the vapor incident angle of the sputtering ions, the sp² hybrid structure increased and the C-Ta bonds contents decreased as a function of the rotational speed, which led to the improvement of adhesion force. The average friction coefficient of the composite coatings did not fluctuate significantly for the amorphous carbon matrix and the transfer films formed during friction, while the wear rates were gradually increased. The sample at 0.5 rpm possessed the lowest wear rate, which was mainly associated with the cooperative behavior of the dense structure and the formation of TaC nanoclusters in the composite coating.

1. Introduction

Amorphous carbon coatings are widely used for the cutting tools, bearing and other moving components as a protection coating owing to their outstanding performances such as high hardness, chemical inertness, outstanding lubrication property and excellent wear resistance [1–3]. However, the coatings normally presented several drawbacks in application and service life, such as high residual stress generated from the deposition and low thermal stability for the metastable sp³C structure. Many methods including doping, and designing multi-layer structure were proposed to solve the problems by tailoring the microstructure of the coatings [4-6]. Goto [7] obtained the Ag-DLC and Cu-DLC coatings with different metal contents by changing the diameter of Ag or Cu tablets in concentric composite target. The tribological results showed that the transition of the friction coefficient became stable when metal-rich tribofilms formed on the counterfaces. Mohammad et al. [8] prepared the soft-hard alternate DLC multilayer coatings above the Cr/CrC_x graded layer by varying the bias voltage during deposition process, and tested the mechanical properties. The results indicated the

multilayer coatings exhibited excellent plastic deformation resistance and adhesion strength.

The microstructure of the sputtering coatings can be adjusted not only by the process design but also by the modification of the deposition parameters. Among the deposition parameters, the substrate rotational speed is one of the most important factors to influence the crystal orientation and structure, as well as the mobility and diffusion of the adsorbed atoms [9,10]. Turkoglu et al. [11] obtained the AZO films by DC magnetron sputtering, and found the substrate rotational speed had a significant influence on the optical, structural and electrical properties. Jayaraman et al. [12] found the homogeneous and preferential orientation of the ZnO films could be modified by the substrate rotational speed. Wada et al. [13] investigated the structure and properties of thermal barrier coatings by changing the substrate rotational speed during deposition. It was found that the substrate rotational speed could tune the growth direction and morphologies of the coatings. Therefore, the structure and properties of the compound coatings or thermal barrier coatings can be reformed by changing the substrate rotational speed during deposition. However, there are not many deep studies regarding

^{*} Corresponding author. State Key Laboratory of Solid Lubrication, Lanzhou Institute of Chemical Physics, Chinese Academy of Science, Lanzhou, 730000, China.

^{**} Corresponding author. State Key Laboratory of Solid Lubrication, Lanzhou Institute of Chemical Physics, Chinese Academy of Science, Lanzhou, 730000, China. E-mail addresses: luyan@licp.cas.cn (Y. Lu), jyhao@licp.cas.cn (J. Hao).

the effect of substrate rotational speed on the microstructure and tribological properties of the amorphous carbon coatings, particularly a-C:metal composite coatings.

In this article, the a-C:Ta composite coatings were prepared on the 9Cr18 steel using physical vapor deposition (PVD) technique by tuning the substrate rotational speed during deposition. The evolutions of the microstructure, hardness, friction and wear behaviors of the a-C:Ta composite coatings were investigated as a function of the substrate rotational speed in detail.

2. Experimental details

2.1. Coatings deposition

The 9Cr18 steel (ϕ 25mm \times 8 mm) was selected as the substrates to test the tribological properties of the coatings for its high hardness. The Si (100) wafers were used to measure the surface morphologies, structure of the carbon bonds and mechanical properties of the coatings. The 9Cr18 steel was polished to achieve a mirror surface. The polished 9Cr18 steel and Si wafers were ultrasonically cleaned in petroleum ether and alcohol for 15 min, respectively.

The magnetron sputtering technique was used to prepare the a-C:Ta composite coatings by controlling the rotation speed of the substrate. The mirror surface of the substrates was faced to the sputtering source with a distance of about 75 mm. The schematic diagram of the deposition process of the composite coatings was shown in Fig. 1. The graphite target and tantalum target with the purity of 99.99% were used as the carbon and Ta source, respectively. The substrates were cleaned for 30 min to remove the oxides contamination on the substrates surface by Ar⁺ bombardments when the pressure reached to 4.0×10^{-4} Pa in the chamber. A buffer layer, which consisted of Cr layer and Cr–C layer, was subsequently deposited on the surface of the substrates to improve the adhesion force. The detailed parameters of the composite coatings during the deposition are shown in Table 1.

2.2. Sample characterization

The field emission scanning electron microscope (FE-SEM JSM-7610F) was used to characterize the cross-section morphologies and thickness of the a-C:Ta composite coatings. The chemical bonds were investigated by Raman spectroscopy (Raman HR Evolution) with an Ar⁺ laser source of 532 nm line. The X-ray photoelectron spectroscopy (XPS ESCALAB 250Xi) was used to analyze the elements binding state, and the source was monochromated Al K α source. The samples used for the XPS test were etched by Ar⁺ for 20 s and then tested in vacuum to avoid the influence of the surface oxides and adventitious carbon. The surface roughness of the coatings was measured by atomic force microscopy (AFM JPK NanoWizard4) with a 2 \times 2 μ m area.

 Table 1

 Detailed parameters of the composite coatings during the deposition.

Films	Target currents (A)			Ar (sccm)	Bias voltage (V)	Substrate rotation speed (rpm)	
	Cr	Ta	С				
Cr	3	0	0	16	400	5	
Cr–C	3	0	3.5	16	60	5	
a-C:Ta-	0	0.2	3.5	16	60	0.5	
a-C:Ta- 2	0	0.2	3.5	16	60	1	
a-C:Ta- 3	0	0.2	3.5	16	60	3	
a-C:Ta- 4	0	0.2	3.5	16	60	5	

The Nano Indenter II system (MTS) was used to measure the hardness and elastic modulus, and the maximum indentation depth was 200 nm to minimize the influence of the 9Cr18 substrate. Each sample was tested for 5 times. The adhesion force between the composite coatings and substrates was tested by the scratch tester (MFT-4000) with a termination loading force of 50 N and a length of 5 mm.

2.3. Friction and wear test

The friction and wear properties were tested under dry sliding condition by a ball-on-disk tribo-meter. The 9Cr18 steel ball with a diameter of 6 mm was selected as the friction counter. The sliding speed of the tribological tests was 0.157 m/s at room temperature, and the total sliding distance was 565 m. The applied load was 5 N and the relative humidity was about 45%.

The morphology and cross-section profiles of the wear tracks were obtained by a 3D surface profiler to calculate the wear rates. The wear tracks of the coatings and the wear scars of the friction pairs were also observed by FE-SEM and EDX (Energy-dispersive X-ray spectroscopy, which was attached to the FE-SEM) to analyze the wear mechanism. The wear volume was measured by the 3D surface profiler, and the wear rate was calculated by the formula [14]: w = V/NS, where w is the wear rate, V is the wear volume, N is the load, and S is the total distance.

3. Results and discussion

3.1. Structure and morphology

The cross-section morphology of the a-C:Ta composite coatings were shown in Fig. 2. The coatings exhibited a dual-layer structure composed of a transition layer and a composite layer with the significant interface, which was caused by the discrepancy of the average atomic mass [15].

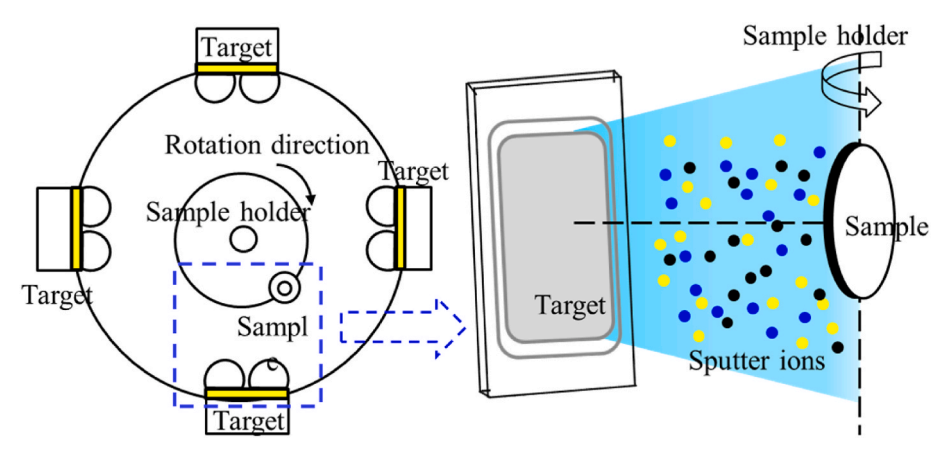


Fig. 1. Schematic diagram of the deposition process of the composite coatings.

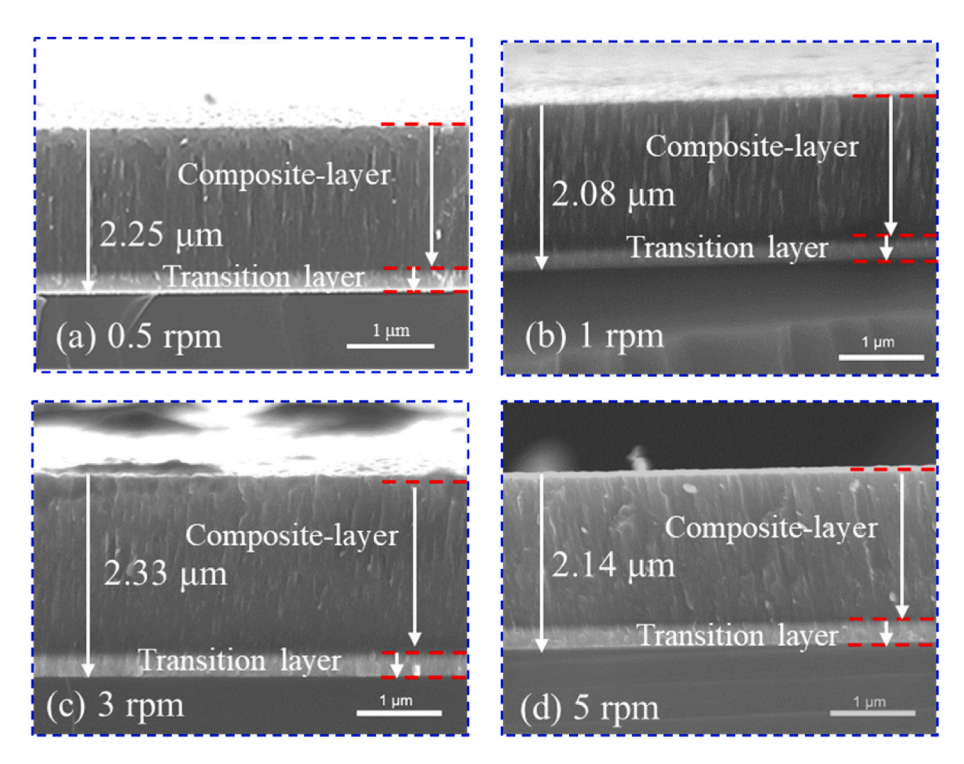


Fig. 2. The cross-section SEM morphologies of the a-C:Ta composite coatings.

The dense coatings transformed into a coarse microstructure with the increase of the substrate rotational speed, due to the incidence state of sputtering ions and the growth interface between the transition layer and the composite layer [16,17]. When the substrate was held at a higher speed, the sputtering ions incidence state of the composite layer was similar with that of the transition layer, hardly changing the growth state and mode of the coatings, resulting in a coarse and columnar structure. However, the growth state and mode were changed when the substrate possessed a lower rotation speed, as the sputtering ions were almost perpendicular to the substrate surface, and thus a dense structure was formed. This result was also described in the earlier studies [18]. Moreover, Wang et al. [19] once obtained a multi-layer coatings at a lower substrate speed during deposition. The multi-layer structure also affected the growth direction and benefited to form a dense structure of the composite coatings.

Another phenomenon that cannot be ignored was the growth direction of the composite layer. The growth direction of the sample at 0.5 rpm was vertical, whereas that of the sample at 5 rpm became obviously inclined. This was related with the vapor incident angle (VIA, Angle between incident direction of sputtering ions and horizontal direction of sample surface). The shadow and lateral migration effect would be

enhanced once the sputtering ions obtained low VIA, resulting in the tilted and coarse morphologies [20,21]. The VIA of most samples at 5 rpm was low, therefore causing the coarse structure.

Fig. 3 showed the AFM results of the samples under different substrate rotational speeds. The roughness and thickness of the coatings first increased and then decreased with the enlargement of the substrate rotational speed that corresponded to the decrease of incident angle. At low rotational speed, the sputtering ions held higher VIA, and the surface rebound and surface injection effect were stronger, which reduced the effective deposition of the sputtering ions on the surface of the substrate, resulting in lower thickness and better surface quality. As the rotational speed increased, the incident angle declined, and the function of the surface rebound and surface injection diminished, so the thickness and the surface roughness increased. With the further increase of the rotational speed, the substrates went farther away from the targets surface, which lowered the energy of sputtering ions due to the combined effect of the particle collision and the magnetic field effect of the target. Such low-energy ions only imposed an etching effect [22] on the coatings and therefore the thickness and the surface roughness decreased again.

Fig. 4a shows the Raman curves of the a-C:Ta composite coatings. It

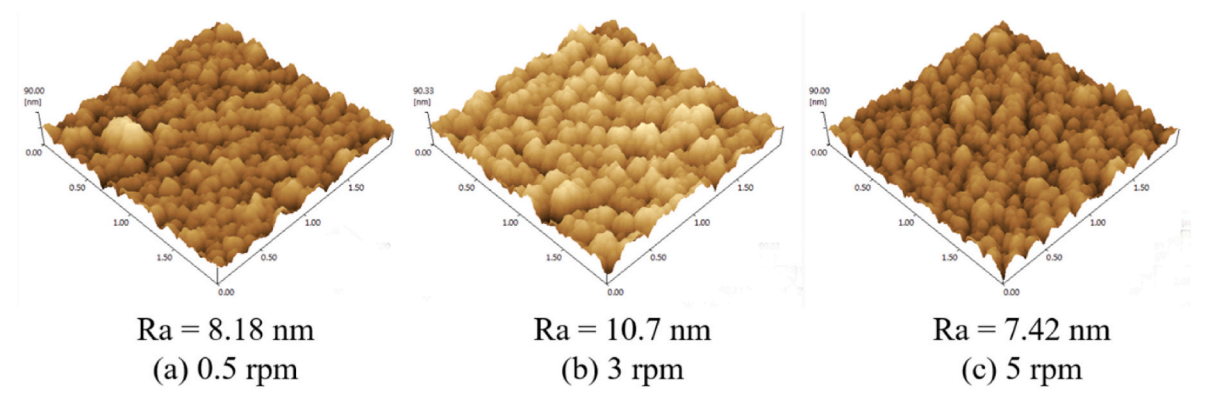


Fig. 3. AFM images of the a-C:Ta composite coatings.

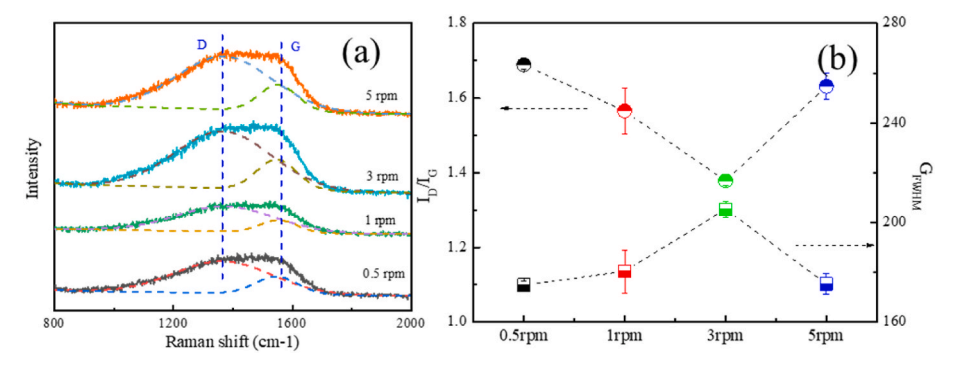


Fig. 4. Raman shift, I_D/I_G and G_{FWHM} of the a-C:Ta composite coatings.

can be seen that the shift of the coatings hardly changed no matter how the substrate rotational speed changed, which implied that the composite coatings were still dominated by amorphous structure. But the intensity of the curves varied, ascribed to the different contents of the centrosymmetric phase (tantalum carbides) in the coatings [23].

The I_D/I_G value and G_{FWHM} were sensitive to the sp^2C content of the carbon-based coatings [24]. The I_D/I_G value showed first decrease and then increase as a function of the substrate rotational speed from Fig. 4b, which demonstrated that the sp^2C contents of the composite coatings decreased at first and then increased. The reasons were related to the tantalum carbides contents and the catalysis of the tantalum clusters. Both of them were decreased with the rotational speed increasing, which led to the decline of the I_D/I_G value. But the VIA were decreased gradually with the increase of the rotational speed and the thermal relaxation phenomenon was enhanced [25], promoting the transition from metastable sp^3C to stable sp^2C . And thus, the re-increase of the I_D/I_G value occurred. The G_{FWHM} exhibited an opposite trend to the I_D/I_G value, which suggested the disorder of the composite coatings was first enlarged and then diminished.

The C 1s spectra of the a-C:Ta composite coatings were shown in

Fig. 5. All the curves could be decomposed into four sub-peaks including C-Ta, sp² C-C, sp³ C-C and C-O by Gaussian fitting [26], which corresponded to the binding energy of 283.1, 284.5, 285.0 and 287.0 eV. The position of the sub-peaks hardly changed for the coatings deposited at various rotational speed, but the C 1s spectra curves fluctuated obviously with the increase in the intensity of C-Ta and decrease in sp² C-C bonds of the composite coatings [27]. The contents of C-M bonds were obtained semi-quantitatively by the area ratios of the C-M bonds to total C 1s peaks. Moreover, the C-Ta bonds contents (the area ratios of the C-Ta bonds and the total C 1s) decreased as a function of the rotational speed, which indicated the tantalum carbides contents declined. Thus the rotational speed played a crucial role in the formation of tantalum carbides in the a-C:Ta composite coatings. The sputtering ions obtained higher VIA and energies at a low rotational speed, and thus the carbon ions could react with tantalum ions to form the tantalum carbides. On the contrary, with the lower VIA and energies of the sputtering ions, the tantalum carbides content decreased at high rotational speed. Moreover, the sp² C-C bonds contents tended to decrease first and then increase with the rotational speed rising, which was in good agreement with the Raman result. XPS results showed that the composite coatings were

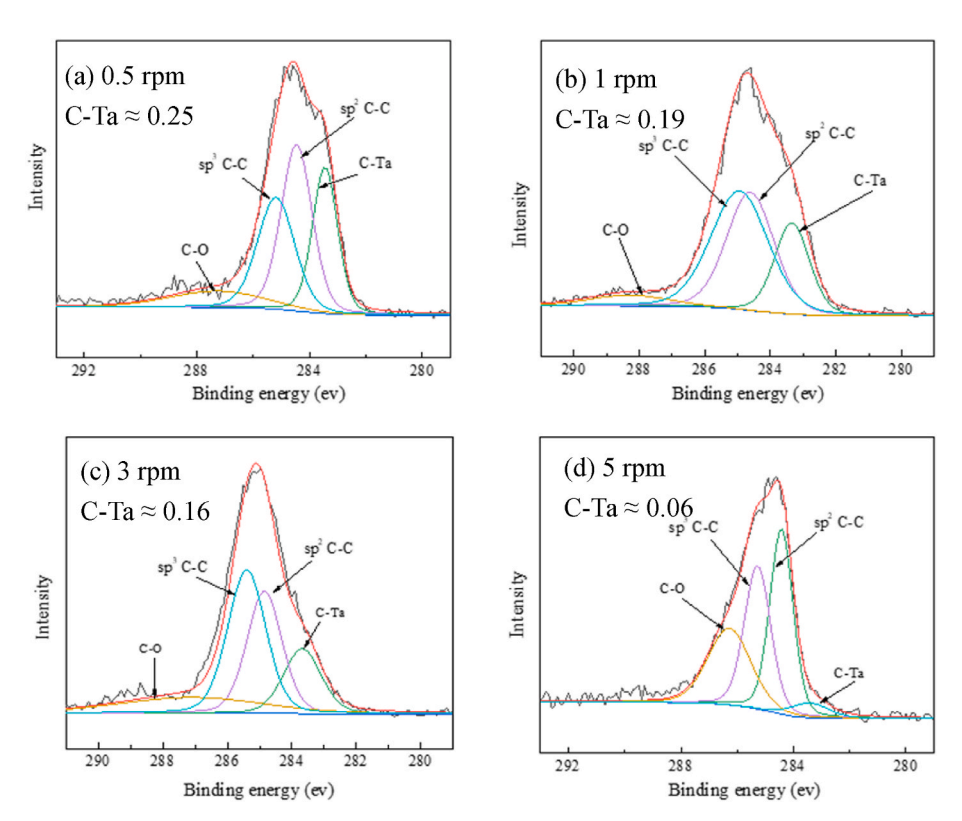


Fig. 5. Deconvolution of C 1s spectra of the a-C:Ta composite coatings.

mainly composed of amorphous carbon, but the structure was intensely affected by the rotational speed during deposition.

The growth state and the microstructure of a-C:Ta composite coatings could be controlled by changing the substrate rotational speed during deposition. However, the energy and density of the sputtering ions were almost similar under the stationary characteristic parameters. Therefore, the main factor affecting the coatings micro-structure was the VIA of the sputtering ions owing to the change of the substrate rotational speed [13,20]. Fig. 6 illustrates the VIA of the sputtering ions in the a-C: Ta composite coatings during deposition. When the VIA of the sputtering ions approached 90°, their abilities to transverse migrate were weak. The surface behaviors of sputtering ions were mainly surface rebound and surface injection. Some ions injected into the subsurface and release the strain energies at the contact sites after the surface action, causing local thermal peak effect and structural relaxation, which resulted in the reduction of compactness and sp³C bonds contents. Some ions directly entered into the subsurface, while the released deformation energies were transformed into the kinetic energy and potential energy of the local ions, increasing the density and sp³C bonds contents [28].

When the sputtering ions were grazing incidence (low VIA), the surface behaviors of sputtering ions were mainly surface migration and surface injection. This could cause the decrease of the ion sub-plantation depth and the increase of transversal migration abilities. According to the sub-implantation model theory [29,30], the higher transversal migration abilities were instrumental for overcoming the energy barriers and reaching to the equilibrium position, which decreased the potential energies of the system. This result promoted the structure relaxation and the transformation from $\rm sp^3C$ bonds to $\rm sp^2C$ bonds, reducing the compactness of the coatings consequently. The normal component energies of the sputtering ions were also decreased under grazing incidence condition, which degenerated the "thermal peak" effect of the coatings. Resultantly, the generated coatings exhibited the high content of high $\rm sp^2C$ bonds and low internal stress.

3.2. Mechanical properties

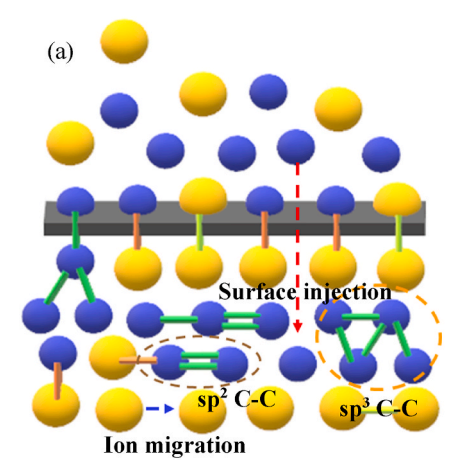
Hardness and elastic modulus are the major indices to evaluate the mechanical properties of the coatings. The hardness and elastic modulus of the a-C:Ta composite coatings as a function of substrate rotational speed were shown in Fig. 7a. Although the hardness of the composite coatings exhibited some fluctuations with the increasing of the substrate rotational speed, the fluctuation was insignificant and it stayed within the experimental error, which meant that the hardness scarcely increased as a function of substrate rotational speed. This can be attributed to the changes in the densities and sp³C contents of the composite coatings [18,31]. Higher sp³C content means higher hardness [32]. As the substrate rotational speed increasing, the I_D/I_G values of the

coatings decreased, resulting in the gradually increase in hardness. While the reduced density of the composite coatings generated to the decrease in hardness. The hard carbide particles (like TaC) in the coatings also involved in regulating the hardness. Those particles played a role in solid-solution strengthening and dispersion strengthening [33], and thus raised the hardness. The 0.5 rpm sample possessed higher carbide content from the XPS results, which increased the hardness. Moreover, some earlier theoretical and experimental studies [10,34] once reported that the carbon coating with higher sp²C bond disorder possessed higher hardness. The coating deposited at 3 rpm exhibited the highest sp²C bond disorder in this study, which favored the enhancement of hardness. The synergistic effect of the reasons above caused the slightly fluctuation in the hardness of the composite coating with the increase of the substrate rotational speed. The elastic modulus stayed nearly constant as a function of the substrate rotational speed due to the amorphous nature of as-deposited coatings [35].

The adhesion force between the substrate and the coating was another important parameter to measure the mechanical properties of the coatings. Fig. 7b shows the friction force and acoustic signal curves during the scratch test of the a-C:Ta composite coatings. Either the friction force or the acoustic signal curves existed a smooth region in the initial stage of the scratch test, followed by some fluctuations. The splitting point between the smooth region and fluctuation region was considered as the critical load (Lc). The critical loads of the coatings monotonically increased as a function of the rotational speed, which was attributed to the change of the Ta-C bond content in the composite coatings. Generally, the bond length is defined as the average nuclear distance between two bonded atoms. Since Ta atom possesses larger atom radium than C atom, the Ta-C bond possesses longer bond length than C-C bond as a consequence. The relationship between the bond length and the adhesion can be explained by the strain. The longer Ta-C bond caused increasing strain as indicated by the shift of the D-peak position in Raman, which made the coatings liable to failure during scratch and consequently premature failure by rupture due to stress concentrations. Such mechanism was also found in the previous study [36-38]. At high rotational speed, the grazing incidence of the sputtering ions and the doped structure of the composite coating could diminish the internal stress and improve the adhesion force.

3.3. Friction and wear properties

Fig. 8a shows the friction curves of the a-C:Ta composite coatings as a function of rotational speed. All the curves could be divided into three stages. In the first stage, the coatings owned higher friction values due to the oxide layer generated on the surfaces of composite coatings and the friction balls. A transfer layer consisting of the graphitized transfer film and physical-chemical reaction film was gradually formed at the friction



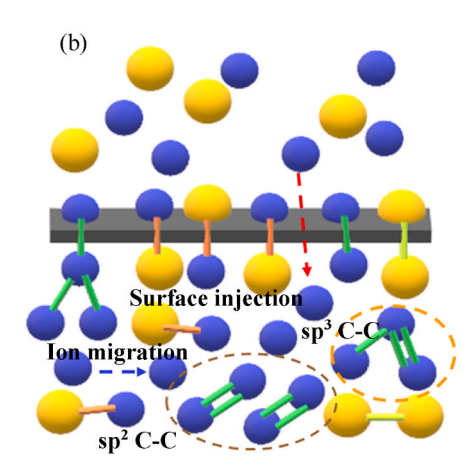


Fig. 6. Schematic diagram of the sputtering ions VIA of the a-C:Ta composite coatings during deposition (a) 0.5 rpm; (b) 5 rpm.

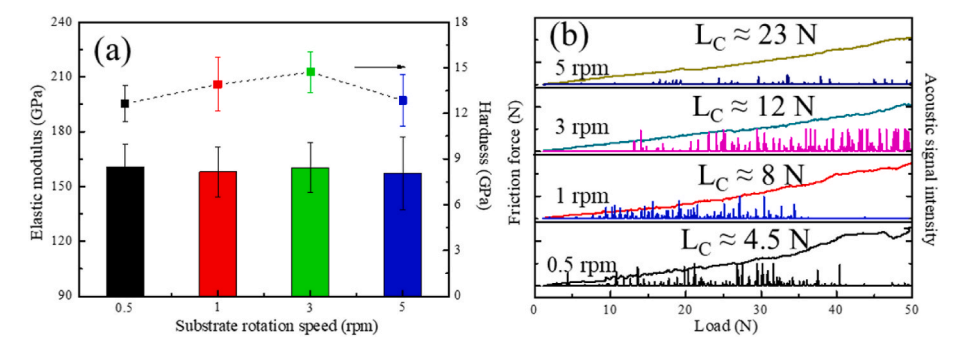


Fig. 7. Mechanical properties of the a-C:Ta composite coatings (a) Hardness and Elastic modulus; (b) Friction force and acoustic signal curves during scratch test.

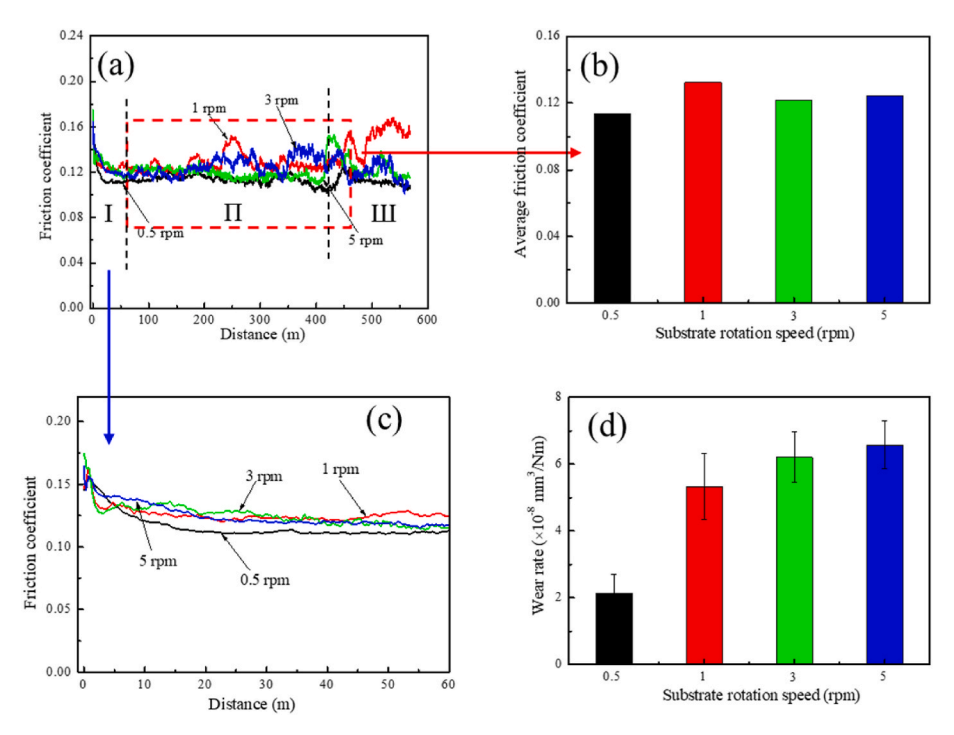


Fig. 8. Tribological properties of the a-C:Ta composite coatings deposited at different rotational speeds (a) Friction curves (b) Average friction coefficient (c) Initial friction curves (d) Wear rates.

interface with the friction going on, which effectively reduced the friction contact area. And thus the friction coefficient values declined [39, 40]. However, the hard particles from the wear debris of the friction balls and coatings could enter into the friction interfaces, imposing the "cutting effect" and damaging the transfer layer, which consequently resulted in the increasing roughness of the friction areas. And the increasing roughness raised the friction coefficient in turn. The friction coefficient then got into the second stage when the formation rate and failure rate of the transfer film reached a dynamic equilibrium. The friction coefficient entered into the third stage when the contact state and roughness of friction surface drastically changed, in which the cutting effect of the hard particles was dominant.

As shown in Fig. 8b, the values of the average friction coefficient of all the composite coatings were stabled at about 0.12, which was connected with the amorphous carbon matrix and the transfer films formed during friction. However, the initial friction coefficient existed obviously difference according to the surface morphologies (shown in Fig. 8c). The VIAs of the sputtering ions were almost 90° at low rotational speed. The surface injection and surface rebound of the ions were the main action states [18,41], improving the compactness and surface quality of composite coatings, which therefore lowered the friction coefficient.

Fig. 8d displays the wear rates of the a-C:Ta composite coatings. At the rotational speed of 0.5 rpm, the composite coating held the lowest wear rate with a value of $2.14 \times 10^{-8} \, \mathrm{mm^3/Nm}$. The composite coating possessed the largest wear rate of $6.57 \times 10^{-8} \, \mathrm{mm^3/Nm}$ at the rotational speed of 5 rpm. Overall, the wear rates of the a-C:Ta composite coatings monotonously increased with the rotational speed increasing. Since the compactness of the microstructure always facilitate the improvement of wear resistance, the monotonous increment of wear rates with increasing the rotational speed was ascribed to the decline of the compactness of the composite coatings. On the other hand, the high carbide content formed at low rotational speed also hindered the crack propagation and improved the wear resistance [42].

The 3D wear topographies and cross-section curves of the a-C:Ta composite coatings deposited at different rotational speeds were shown in Fig. 9. Obvious furrows could be observed in all the wear tracks of the a-C:Ta composite coatings, which indicated the abrasive wear was the main wear mechanism. The furrows of the contact areas gradually aggravated with the increase of the rotational speed, which could increase the roughness and friction coefficient of the composite coatings during friction. Moreover, the depth and width of the wear tracks also increased with the increase of the rotational speed. This was because the multi-layer interfaces of the composite coating formed at low rotational

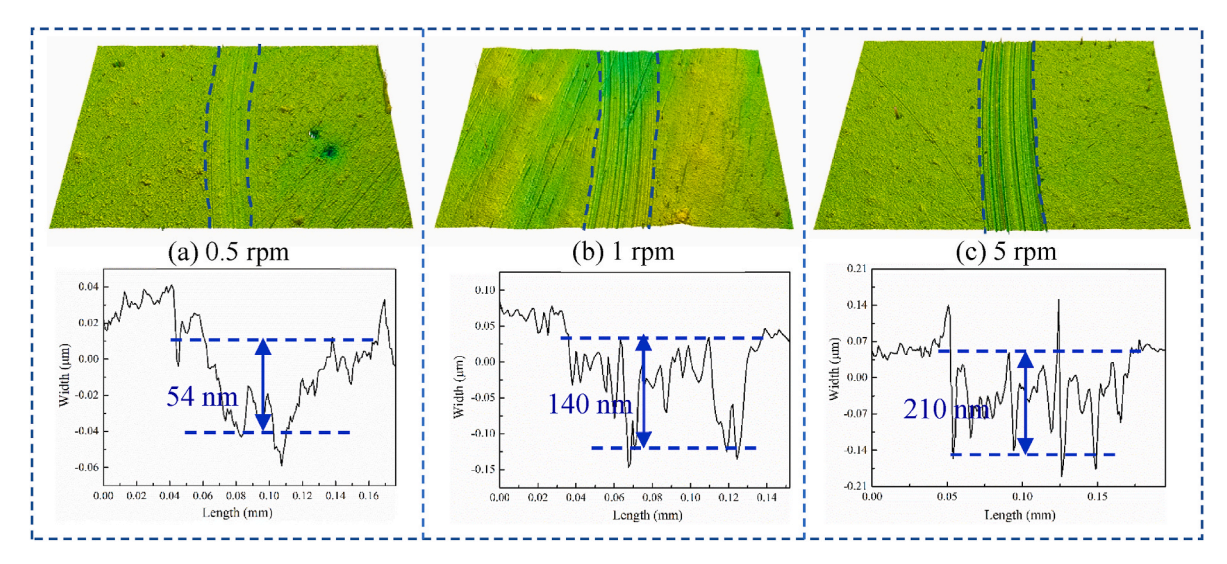


Fig. 9. 3D wear topographies and cross-section curves of the a-C:Ta composite coatings deposited at different rotational speeds.

speed could resist the cutting effect of hard particles, which effectively diminished the depth and width of the wear tracks. The cutting effect was dominant at high rotational speed for the coarser structure and lower hardness, which aggravated the wear.

The SEM morphologies of the wear tracks and wear scars of the a-C: Ta composite coatings deposited at different rotational speeds were shown in Fig. 10. The wear track of sample at 0.5 rpm was light and shallow, while the wear debris were hardly observed. However, the wear track of sample at 5 rpm was deep and wide, with containing more wear debris contained. This can be explained by the low compactness of the sample at 5 rpm. The incompact microstructure was prone to cracking under the tangential force and weakening the shear resistance of the sample [33], resulting in the generation of massive wear debris and serious wear. The dense structure of the sample at 0.5 rpm can eliminate the initiation and propagation of cracks and thus the wear resistance was improved. Another reason for the improvement of the wear resistance was the formation of tantalum carbide in the composite coatings. These

carbides can be dispersed in the amorphous carbon coatings, acting as "dispersion strengthening" and "solid-solution strengthening" agent [43,44], to enhance the wear resistance. The sample at 0.5 rpm possessed higher content of C–Ta bonds than the sample at 5 rpm from the XPS results, which implied the sample at 0.5 rpm had higher anti-wear property.

By comparison of the wear scars in Fig. 10c and d, the smaller wear scar at 0.5 rpm implied smaller friction contact area, which was conducive to reduce the friction coefficient (Fig. 8b). The existence of transfer films can be observed in both wear scars, indicating the graphitization of the composite coatings during friction [45,46]. And this was also instrumental in reducing the friction coefficient.

Table 2 shows the EDX results of the points in Fig. 10. The presence of O element indicated that the oxidation reaction occurred during the friction, which originated from the reaction between the oxygen in the air and the steel ball due to the higher friction flash temperatures, generating the oxides (such as Cr_2O_3) with higher hardness. Those hard

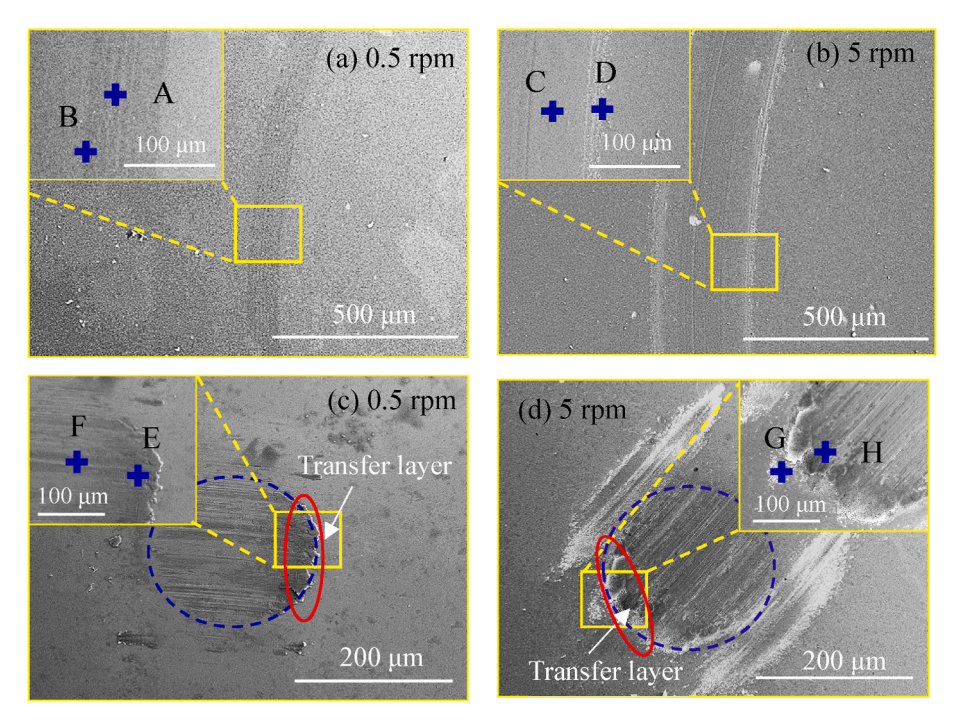


Fig. 10. SEM morphologies of the wear tracks and wear scars of the a-C:Ta composite coatings deposited with different rotational speeds.

Table 2The elements analyzed for the point of Fig. 10 at%.

Point	С	O	Cr	Fe	Ta
A	$\textbf{83.2} \pm \textbf{2.2}$	1.0 ± 0.1	9.3 ± 0.8	3.0 ± 1.3	3.6 ± 0.1
В	71.6 ± 1.3	$\textbf{8.7} \pm \textbf{0.5}$	9.8 ± 1.3	5.7 ± 0.8	4.3 ± 0.3
C	$\textbf{85.3} \pm \textbf{2.6}$	1.9 ± 0.5	6.9 ± 1.6	2.4 ± 0.7	3.6 ± 0.8
D	51.0 ± 3.2	33.8 ± 3.8	3.0 ± 0.5	8.4 ± 0.7	$\textbf{7.8} \pm \textbf{0.5}$
E	17.4 ± 1.4	40.1 ± 3.1	7.3 ± 0.9	27.5 ± 3.1	$\textbf{7.8} \pm \textbf{0.5}$
F	5.2 ± 1.5	0.6 ± 0.2	12.9 ± 1.1	81.0 ± 2.2	$\textbf{0.4} \pm \textbf{0.2}$
G	11.8 ± 1.6	41.0 ± 1.5	$\textbf{7.8} \pm \textbf{1.0}$	35.8 ± 1.7	3.5 ± 0.8
Н	51.8 ± 2.0	15.9 ± 1.8	12.5 ± 1.4	17.9 ± 1.5	1.9 ± 0.8

particles consisting of Cr_2O_3 and TaC scratched the coatings surface and formed the furrows, contributing to the changes in the friction coefficient and the wear rate.

It is worth noting that there was some variation in the composition of each point, whether it was in the wear tracks or the wear scars. The variation in the composition of each point was related to the degree of oxidation reaction, graphitization transfer film and the component changes of the wear abrasive. For the wear tracks, all of the points possessed higher carbon atoms content, which was attributed to the amorphous carbon matrix. The points of B and D were provided with higher oxygen content due to the variation in the degree of oxidation reaction. The distinct contents of wear debris from steel ball led to the different contents of Fe, and Cr in the points. As to the wear scars, the graphitization transfer films formed during friction were generated and assembled along the friction direction by the cutting force, which led to higher C contents (point E and H). The embedded wear debris from the steel ball contributed to the lower contents of Fe and Cr. The lower carbon content and higher Fe and Cr contents in the friction contact area (point F) resulted from the thin graphitization transfer film (which can be penetrated by X ray). The variation in elemental content at point G was related to the amount of the mixture of graphitization transfer film and the wear abrasive from the steel ball.

4. Conclusion

The a-C:Ta composite coatings were papered by tailoring the substrate rotational speed during deposition in this study. The structure of the coatings gradually changed from dense structure to columnar structure with the increase of the rotational speed. Moreover, the growth direction of the composite coatings changed from vertical to inclined direction due to the change of the VIA of the sputtering ions. It was also found that increasing the rotational speed inhibited the formation of C-Ta bonds and contributed to the improvement of adhesion force between the substrate and composite coatings. The hardness and elastic modulus staved nearly constant as a function of the substrate rotational speed, which was connected with the carbide content and disorder of sp²C bonds. The tribological investigations demonstrated that the volatility of friction coefficient was closely related to the surface roughness and the formation rate of the transfer layer, while the wear rate was greatly affected by the compactness and the content of metal carbides. The dominant wear mechanism in the composite coatings was abrasive wear. The lowest wear rate appeared at 0.5 rpm, benefiting from the dense microstructure and the high carbide contents of the composite coating.

Declaration of competing interest

The authors declare that they have no known competing financial interests or personal relationships that could have appeared to influence the work reported in this paper.

Acknowledgments

The authors gratefully acknowledge the financial support of the

National Natural Science Foundation of China (51835012, 51975554), the Natural Science Foundation of Gansu Province (21JR7RA091), Basic Research Project (2020-JCJQ-ZD-155-12).

References

- Š. Meškinis, S. Tamulevičius, Diamond-like carbon based silver nanocompositesshort review of the technology and novel applications, Physics, Chemistry and Applications of Nanostructures (2015).
- [2] M. Ghasemi, B. Ghasemi, H. Semnani, M. Erfanmanesh, A comparative study of duty cycle and argon/methane flow ratio effect on the tribological behavior of DLC coatings over nitrided Astaloy Mo-based steel, Ceram. Int. 47 (2021) 12467–12475.
- [3] K. Mahmud, M. Kalam, H. Masjuki, H. Mobarak, N. Zulkifli, An updated overview of diamond-like carbon coating in tribology, Crit Rev Solid State 40 (2015) 90–118.
- [4] L. Patnaik, R. Saikat, K. Sunil, Comprehensive structural, nanomechanical and tribological evaluation of silver doped DLC thin film coating with chromium interlayer (Ag-DLC/Cr) for biomedical application, Ceram. Int. 14 (2020) 22805–22818.
- [5] S. Bhowmick, A. Banerji, A. Alpas, Friction reduction mechanisms in multilayer graphene sliding against hydrogenated diamond-like carbon, Carbon 109 (2016) 795–804
- [6] I. CastilloMüller, J. Sharp, W. Rainforth, P. Hovsepian, A. Ehiasarian, Tribological response and characterization of Mo-W doped DLC coating, Wear 376 (2017) 1622–1629.
- [7] M. Goto, Preparations and tribological properties of soft-metal/DLC composite coatings by RF magnetron sputter using composite targets, Int. J. Mech. Mater. Des. 14 (2018) 313–327.
- [8] S. Mohammad, Z. Zhou, Z. Xie, P. Munroe, Designing multilayer diamond like carbon coatings for improved mechanical properties, J. Mater. Sci. Technol. 65 (2021) 108–117.
- [9] N. Panich, Y. Sun, Effect of substrate rotation on structure, hardness and adhesion of magnetron sputtered TiB₂ coating on high speed steel, Thin Solid Films 2 (2006) 190–196.
- [10] J. Jiang, Q. Wang, H. Huang, Y. Wang, X. Zhang, J. Hao, Microstructure and property changes induced by substrate rotation in titanium/silicon dual-doped a-C: H films deposited by mid-frequency magnetron sputtering, Surf. Coating. Technol. 240 (2014) 419–424.
- [11] F. Turkoglu, H. Koseoglu, S. Zeybek, M. Ozdemir, G. Aygun, L. Ozyuzer, Effect of substrate rotation speed and off-center deposition on the structural, optical, and electrical properties of AZO thin films fabricated by DC magnetron sputtering, J. Appl. Phys. 123 (2018), 165104.
- [12] V. Jayaraman, M. Yasuhiro, M. Arturo, Importance of substrate rotation speed on the growth of homogeneous ZnO thin films by reactive sputtering, Mater. Lett. 169 (2016) 1–4
- [13] K. Wada, Y. Norio, M. Hideaki, Effect of substrate rotation on texture evolution in ZrO₂-4 mol.% Y₂O₃ layers fabricated by EB-PVD, Surf. Coating. Technol. 191 (2005) 367–374.
- [14] X. Sui, R. Xu, J. Liu, S. Zhang, Y. Wu, J. Yang, J. Hao, Tailoring the tribocorrosion and antifouling performance of (Cr, Cu)-GLC coatings for marine application, ACS Appl. Mater. Interfaces 42 (2018) 36531–36539.
- [15] M. Yan, X. Sui, X. Wang, S. Zhang, Y. Lu, J. Hao, W. Liu, Construction of a dense structure for GLC coatings by tailoring the nitrogen content to improve the aqueous-adaptability, Surf. Coating. Technol. 418 (2021), 127131.
- [16] M. Joe, M. Moon, J. Oh, K. Lee, K. Lee, Molecular dynamics simulation study of the growth of a rough amorphous carbon film by the grazing incidence of energetic carbon atoms, Carbon 50 (2012) 404–410.
- [17] J. Cho, S. Terry, R. LeSar, C. Levia, A kinetic Monte Carlo simulation of film growth by physical vapor deposition on rotating substrates, Mater. Sci. Eng. 391 (2005) 390–401.
- [18] M. Matsumoto, K. Wada, N. Yamaguchi, T. Kato, H. Matsubara, Effects of substrate rotation speed during deposition on the thermal cycle life of thermal barrier coatings fabricated by electron beam physical vapor deposition, Surf. Coating. Technol. 202 (2008) 3507–3512.
- [19] W. Wang, L. Ji, H. Li, X. Liu, H. Zhou, J. Chen, Influence of rotational speed on structure, mechanical and electrical properties of TiC/GLC composite films, Diam. Relat. Mater. 92 (2019) 65–73.
- [20] T. Ma, Y. Hu, H. Wang, Growth mechanism of diamond-like carbon film based on the simulation model of atomic motion, Acta Phys Sin-ch. 56 (2007) 480–486.
- [21] J. Robertson, Deposition mechanisms for promoting sp³ bonding in diamond-like carbon, Diam. Relat. Mater. 2 (1993) 984–989.
- [22] N. Derradji, M. Mahdjoubi, H. Belkhir, N. Mumumbila, B. Angleraud, P. Tessier, Nitrogen effect on the electrical properties of CNx thin films deposited by reactive magnetron sputtering, Thin Solid Films 482 (2005) 258–263.
- [23] A. Wang, K. Lee, J. Ahn, J. Han, Structure and mechanical properties of W incorporated diamond-like carbon films prepared by a hybrid ion beam deposition technique, Carbon 44 (2006) 1826–1832.
- [24] A. Ferrari, Raman spectroscopy of graphene and graphite: disorder, electronphonon coupling, doping and nonadiabatic effects, Solid State Commun. 143 (2007) 47–57.
- [25] T. Ma, Y. Hu, H. Wang, Role of atomic transverse migration in growth of diamond-like carbon films, Chin. Phys. B 16 (2007) 2798–2802.

- [26] M. Vargas, H. Castillo, E. Restrepo-Parra, L. De, Stoichiometry behavior of TaN, TaCN and TaC thin films produced by magnetron sputtering, Appl. Surf. Sci. 279 (2013) 7–12.
- [27] G. Greczynski, L. Hultman, X-ray photoelectron spectroscopy: towards reliable binding energy referencing, Prog. Mater. Sci. 107 (2019), 100591.
- [28] P. Kelires, Energetics and stability of diamondlike amorphous carbon, Phys. Rev. Lett. 68 (1992) 1854.
- [29] J. Robertson, Diamond-like amorphous carbon, Mater. Sci. Eng. R Rep. 37 (2002) 129–281.
- [30] Y. Lifshitz, G. Lempert, E. Grossman, Substantiation of subplantation model for diamond like film growth by atomic force microscopy, Phys. Rev. Lett. 72 (1994) 2753
- [31] L. Wang, L. Li, X. Kuang, Effect of substrate bias on microstructure and mechanical properties of WC-DLC coatings deposited by HiPIMS, Surf. Coating. Technol. 352 (2018) 33–41.
- [32] F. Shahsavari, M. Ehteshamzadeh, M. Amin, A. Barlow, A comparative study of surface morphology, mechanical and tribological properties of DLC films deposited on Cr and Ni nanolayers, Ceram. Int. 46 (2020) 5077–5085.
- [33] Y. Zhou, L. Li, W. Shao, Z. Chen, S. Wang, X. Xing, Q. Yang, Mechanical and tribological behaviors of Ti-DLC films deposited on 304 stainless steel: exploration with Ti doping from micro to macro, Diam. Relat. Mater. 107 (2020), 107870.
- [34] T. Kumagai, S. Sawai, J. Choi, S. Izumi, T. Kato, Nanostructural interpretation for elastic softening of amorphous carbon induced by the incorporation of silicon and hydrogen atoms, J. Appl. Phys. 107 (2010), 710-146.
- [35] M. Berdova, X. Liu, C. Wiemer, A. Lamperti, G. Tallarida, E. Cianci, M. Fanciulli, S. Franssila, Hardness, elastic modulus, and wear resistance of hafnium oxidebased films grown by atomic layer deposition, J. Vac. Sci. Technol., A 34 (2016), 051510.
- [36] Y. Xiao, W. Sun, Y. Zhang, Y. Jia, J. Liu, C. Zhang, Electrodeposition, Microstructure and Tribological Performance of Ni/(N) Incorporated Diamond-like Carbon Films, vol. 447, 2022, 128876.

- [37] Y. Zhang, W. Sun, Y. Dong, M. Ma, Y. Liu, S. Tian, Y. Xiao, Y. Jia, Electrodeposition and microstructure of Ni and B co-doped diamond-like carbon (Ni/B-DLC) films, Surf. Coating. Technol. 405 (2021), 126713.
- [38] N. Khun, E. Liu, X. Zeng, Corrosion behavior of nitrogen doped diamond-like carbon thin films in NaCl solutions, Corrosion Sci. 51 (2009) 2158–2164.
- [39] J. Wang, K. Zhang, L. Zhang, F. Wang, J. Zhang, W. Zheng, Influence of structure evolution on tribological properties of fluorine-containing diamond-like carbon films: from fullerene-like to amorphous structures, Appl. Surf. Sci. 457 (2018) 388-305
- [40] H. Kovacı, A. Yetim, Ö. Baran, A. Çelika, Tribological behavior of DLC films and duplex ceramic coatings under different sliding conditions, Ceram. Int. 44 (2018) 7151–7158.
- [41] Y. Yamada, M. Murashima, N. Umehara, T. Tokoroyama, W. Lee, H. Takamatsu, Y. Tanaka, Y. Utsumi, Effect of fracture properties and surface morphology on wear of DLC coatings at severe contact condition, Tribol. Int. 169 (2022), 107486.
- [42] C. Liang, W. Wang, C. Huang, H. Tsai, C. Yang, The influence of microstructural variations on mechanical and tribological properties of low-friction TiC/diamondlike carbon nanocomposite films, Ceram. Int. 40 (2014) 13329–13337.
- [43] J. Solis, H. Zhao, C. Wang, J. Verduzco, A. Bueno, A. Neville, Tribological performance of an H-DLC coating prepared by PECVD, Appl. Surf. Sci. 383 (2016) 222–232.
- [44] D. Xiang, X. Tan, X. Sui, J. He, C. Chen, J. Hao, Z. Liao, W. Liu, Comparative study on microstructure, bio-tribological behavior and cytocompatibility of Cr-doped amorphous carbon films for Co-Cr-Mo artificial lumbar disc, Tribol. Int. 155 (2021), 106760.
- [45] X. Liu, N. Umehara, T. Tokoroyama, M. Murashima, Tribological properties of ta-CNx coating sliding against steel and sapphire in unlubricated condition, Tribol. Int. 131 (2019) 102–111.
- [46] W. Koszela, P. Pawlus, R. Reizer, T. Liskiewicz, The combined effect of surface texturing and DLC coating on the functional properties of internal combustion engines, Tribol. Int. 127 (2018) 470–477.